ADVANCED FUNCTIONAL MATERIALS
www.afm-journal.de

www.MaterialsViews.com

High-Performance Thermally Stable Organic Phototransistors Based on PSeTPTI/$PC_{61}BM$ for Visible and Ultraviolet Photodetection

Zhe Qi, Jiamin Cao, Hui Li, Liming Ding,* and Jizheng Wang**

Phototransistors are three-terminal photodetectors which usually have higher photosensitivity than photodiodes due to the presence of gate electrode. In this report, organic phototransistors (OPTs) based on a donor material, namely, poly{2,5-selenophene-alt-2,8-(4,10-bis(2-hexyldecyl))thieno[2′,3′:5,6]-pyrido[3,4-*g*]thieno[3,2-*c*]isoquinoline-5,11(4*H*,10*H*)-dione} (PSeTPTI), are fabricated and intensively studied. As unipolar p-type organic semiconductor usually has plenty of electron traps in the bulk to impede electron transporting, most of photogenerated electrons will fill the traps in PSeTPTI and this process can prolong the response time. By introducing [6,6]-phenyl C_{61} butyric acid methyl ester on top, the p–n heterojunction can produce most of the photocurrent and eliminates the influence from the process of trapping electrons. This mechanism improves the photoresponsivity and response speed. Since ultraviolet (UV) detection is very important in some fields including military, aerospace, and biology, the OPTs are characterized under UV illumination besides the visible light and they present high sensitivity. Furthermore, organic semiconductors often have bad stability in harsh conditions and meanwhile some devices need to work in these environments. At high temperature even up to 200 °C, our OPTs can work normally and show very high stability, indicating the potential of the devices in applications of high-temperature environments.

1. Introduction

With tremendous developments of molecular design and processing technique, organic filed-effect transistors (OFETs) are becoming a more and more competitive candidate for applications like radio frequency identification (RFID) tags, smart cards, and active matrix displays.[1–5] Besides functioning as a logic switch, multiple functions are developed for OFETs such as light-emitting devices, memory cells, and sensors.[6–8] By virtue of chemical versatility, the optoelectronic features of organic materials are easily tuned and organic semiconductors usually display high light absorption coefficient.[9–12] Thus, OFETs-based light sensors namely organic phototransistors (OPTs) are attracting researchers' attention more and more.[13–17] Compared with light sensors that have two terminals, phototransistors enable easier control of light-detection sensitivity without problems such as the noise increment due to the additional gate terminal.[13] For thin-film OPTs, Noh et al. fabricated OPTs based on 2,5-bis-biphenyl-4-yl-thieno[3,2-b]thiophene (BPTT) with maximum responsivity (R) of 82 A W^{-1}.[18] Poly(3-hexylthiophene) (P3HT) based OPTs showed R of 245 A W^{-1},[19] poly(9,9-dioctylfluorene-co-bithiophene) (F8T2) and poly(3,3‴-didodecylquarterthiophene) (PQT-12) based OPTs showed R of 18.5 and 6.6 A W^{-1}.[20,21] Recently, Joo and co-workers reported a high R of 2500–4300 A W^{-1} with a star-shaped molecule 1,2,4,5-tetra(5′-hexyl-[2,2′]-bithiophenyl-5-vinyl)-benzene (4(HPBT)-benzene).[15] Single crystal OPTs always present higher responsivity due to the low trap density and fast charge transport. With 6-methyl-anthra[2,3-b]benzo[d] thiophene (Me-ABT) microribbon, the OPTs display high R of 12 000 A W^{-1}.[14] OPTs with single crystal anthracene-2-ethynyl-5-hexyldithieno[3,2-b:2′,3′-d]thiophene (A-EHDTT) present R of 1.4×10^4 A W^{-1}.[17] However, though owning higher performance, the single crystal OPTs are not fit for the low-cost large-scale fabrication. Thus, developing thin-film OPTs is more desirable. Moreover, response time of OPTs is less studied although these characteristics are very important in practical photosensing applications. It is necessary to investigate and improve the response time in OPTs for further enhancing the performance.

For wavelength of photodetection, ultraviolet (UV) region holds an important position as UV detection can be applied in fields like chemical sensing, military application, ozone sensing, and missile warning.[22,23] We performed UV photoresponse test besides the visible light detection. Our OPTs present maximum R as high as 2.2×10^4 A W^{-1} under UV illumination. Since some

Z. Qi, Dr. H. Li, Prof. J. Wang
Beijing National Laboratory for Molecular Sciences
Key Laboratory of Organic Solids
Institute of Chemistry
Chinese Academy of Sciences
Beijing 100190, P.R. China
E-mail: jizheng@iccas.ac.cn; lihui@iccas.ac.cn
Z. Qi
University of Chinese Academy of Sciences
Beijing 100049, P.R. China
J. Cao, Prof. L. Ding
National Center for Nanoscience and Technology
Beijing 100190, P.R. China
E-mail: ding@nanoctr.cn

DOI: 10.1002/adfm.201500525

special conditions require stable devices capable of working in harsh environments such as at high temperature, it is important to discuss whether organic based photodetectors can qualify under such stringent conditions, especially in consideration that organic semiconductors always show instable performance at high temperature. So stably working OPTs under high-temperature conditions are useful but challenging. We performed a photoresponse test of OPTs working at high temperature up to 200 °C and the OPTs present very good stability. This result indicates that even though under such stringent conditions of 200 °C, our OPTs can work normally and stably.

2. Results and Discussion

2.1. OFETs

Inset of **Figure 1**a presents the chemical structure of poly{2,5-selenophene-alt-2,8-(4,10-bis(2-hexyldecyl))thieno[2′,3′:5,6]-pyrido[3,4-*g*]thieno[3,2-*c*]isoquinoline-5,11(4*H*,10*H*)-dione} (PSeTPTI). With selenophene instead of thiophene, the molecular acquires enhanced planarity, extended conjugation length, and reduced bandgap.[24] Selenium is more polarizable than sulfur, Se–Se interactions favor interchain charge hopping and increase hole mobility.[25] With these features, PSeTPTI can be a good hole transporting material. In previous report, PSeTPTI/[6,6]-phenyl C71 butyric acid methyl ester (PSeTPTI/PCBM) solar cells showed PCE of 6.04%, indicating that PSeTPTI/PCBM can form a wonderful p–n heterojunction.[26] Figure 1a shows the absorption spectra of spin-coated PSeTPTI film, in which the material displays wide light absorption in visible and UV region indicating its potential for visible and UV photodetection.

We utilized this donor material PSeTPTI to fabricate our devices. The OFET performance is shown in Figure 1b,c. The device shows standard transfer and output curves with hole mobility of 0.12 $cm^2 V^{-1} s^{-1}$, threshold voltage of –8.75 V, and an on/off ratio of 1.43×10^8. The off current can be below 10^{-12} A, which can offer high photosensitivity in photodetection. It should be noted that the fabrication and characterization were performed under ambient conditions. The device was intentionally tested for multiple times and showed stable transfer curves (Figure 1b). It is vital that devices have a stable dark state for acting as light sensors. Figure 1d shows the on/off current cycle curve, and the on current at –80 V and off current at 20 V display little deterioration after 1 h circulation indicating the good electrical stability of the device. Through the characterizations above, the material presents wide light absorption from UV to visible region and the fabricated device shows excellent OFET performance, dark stability, and electrical stability. These characteristics can offer the basic preconditions to be light sensors.

2.2. $PC_{61}BM$ Enhanced Visible Photodetection

First, the pure-PSeTPTI based OPTs were investigated. The photoresponse behavior was characterized and the results are displayed in **Figure 2**. When the OPT is exposed to the white light, the I_{DS} increases dramatically because the absorbed photons generate charge carriers to boost the current (Figure 2a). From the transfer curves in the dark and under illumination, we calculated two important parameters of OPTs, namely, *R* and

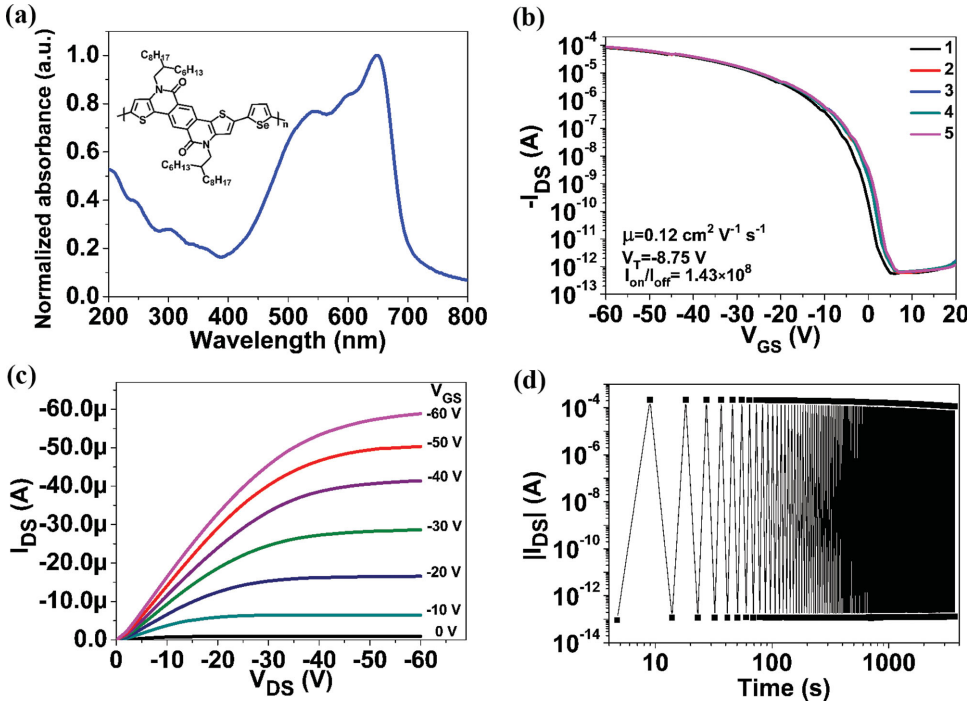

Figure 1. a) Chemical structure and absorption spectra of PSeTPTI. b,c) Transfer and output curves of pure PSeTPTI based OFET under ambient conditions (V_{DS} = –60 V, W = 1400 μm, L = 10 μm). d) The on/off current cycle testing for 1 h (V_{DS} = –60 V, V_{GS} = 20 V, or –80 V).

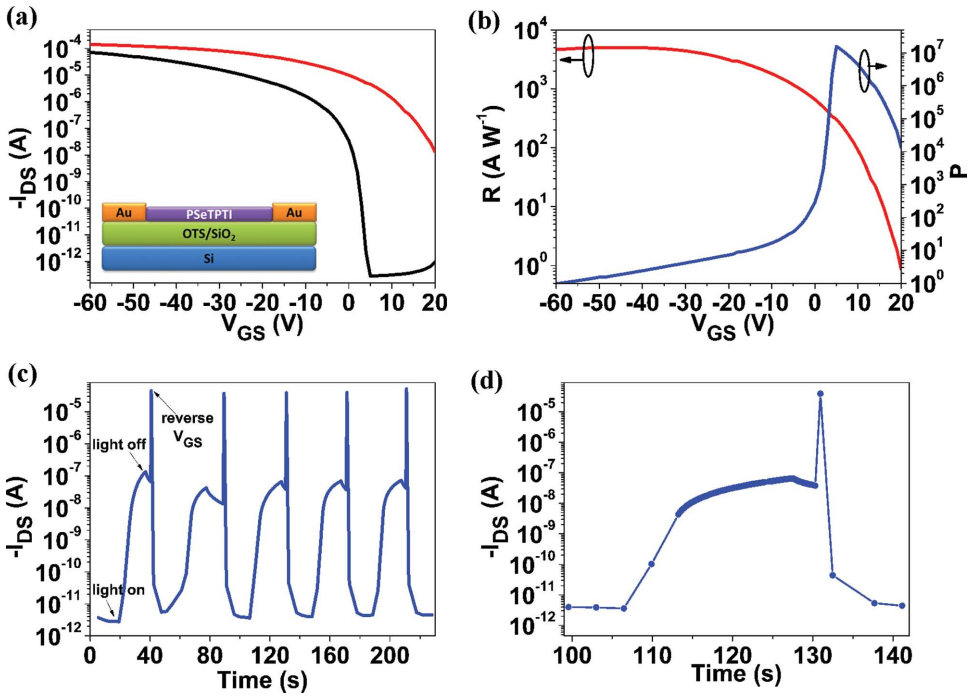

Figure 2. a) Transfer curves of pure PSeTPTI based OPT in the dark and under white light illumination (107 μW cm^{-2}). Inset: device structure of the OPT. b) R and P as a function of V_{GS}. c) The real-time I_{DS} change under dynamic photoswitching on/off (V_{GS} = 10 V, V_{DS} = −60 V). d) One transient photoresponse.

photocurrent/dark-current ratio (P), based on the following fundamental equations[13]

$$R = \frac{I_{ph}}{P_{inc}} = \frac{I_{light} - I_{dark}}{P_{inc}} \quad (1)$$

$$P = \frac{I_{ph}}{I_{dark}} = \frac{I_{light} - I_{dark}}{I_{dark}} \quad (2)$$

where I_{light} is the drain current under illumination, I_{dark} is the drain current in the dark. P_{inc} is the incident illumination power on the channel area. The R and P versus V_{GS} curves are shown in Figure 2b. At the cross point of two curves (V_{GS} = 3.2 V), the R and P are 362 A W^{-1} and 1.1 × 10^5, respectively. To demonstrate the real-time photoresponse, the change of I_{DS} with repeated photo on/off switching was characterized. As can be seen from Figure 2c, the device displays reproducible photosensing behavior. In every photoresponse cycle, the persistent photoconductivity (PPC) was observed.[15,27,28] The PPC phenomenon signifies that the I_{DS} declines very slowly and maintains a high current value for a long time even after the light is off. This is probably because the trapped photoelectrons which recombine tardily and live long slower the recovery of the current. Thus, an additional negative gate voltage pulse (–80 V, the peak value point in every cycle) which can drive the recombination forcefully is needed to erase the photomemory effect. On the other hand, each photoresponse cycle is just like an erasable memory operation. That is the "write" operation (light on), the "read-on" operation (the on-state current maintains due to the PPC), the "erase" operation (negative gate voltage pulse), and the "read-off" operation (the off-state current after erasing). This offers multifunction combining memory device and photosensing. In one transient photoresponse, it takes long time for the I_{DS} to reach maximum value after switching on the light and the rise time (defined as the time for the current to rise to 90% of the maximum value) is as long as 19.4 s (Figure 2d). In this OPT, the semiconductor is only good for transporting holes, but bad for transporting electrons as there are a lot of electron traps in the bulk. Under illumination, the photogenerated holes transport to the drain electrode quickly, but the photogenerated electrons will fill in the electron traps of the p-type material resulting in prolonged lifetime of photogenerated electrons. To keep the neutrality of the semiconductor, each hole reaching the drain is replenished by another entering from the source.[28] This is the gain mechanism due to the increased lifetime of photogenerated electrons. That means more trapped electrons will lead to larger gain and larger current. But, because the process for photogenerated electrons to fill in traps until saturation extent requires long time, the rise speed becomes slow. The long rise time not only influences the response speed but also the on-current (the maximum current after switching on the light in the real-time test).

Then, we introduced PSeTPTI/[6,6]-phenyl C_{61} butyric acid methyl ester ($PC_{61}BM$) heterojunction trying to improve the OPTs above. 3 nm $PC_{61}BM$ (the thickness was obtained from thickness monitor of vacuum evaporation system) was deposited on top of PSeTPTI film by thermal evaporation. We utilized the same device to make a convictive comparison. The photoresponse performance is displayed in **Figure 3**. In the dark, the transfer curve is similar to that of original pure-PSeTPTI based OPT (Figure 3a). Under illumination of the

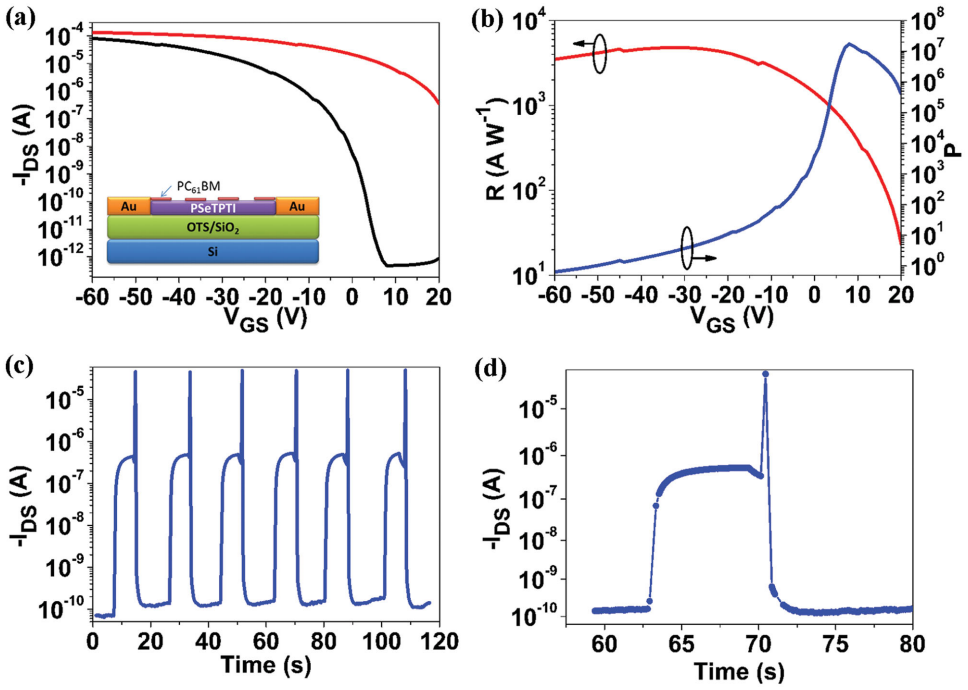

Figure 3. a) Transfer curves of $PC_{61}BM$ deposited OPT in the dark and under white light illumination (107 μW cm^{-2}). Inset: device structure of this OPT. b) *R* and *P* as a function of V_{GS}. c) The real-time I_{DS} change under dynamic photoswitching on/off (V_{GS} = 10 V, V_{DS} = −60 V). d) One transient photoresponse.

same power density, the current is larger than that of original OPT in the depletion region. At the cross point (V_{GS} = 3.5 V), *R* and *P* reach as high as 1010 A W^{-1} and 2.3×10^5 (Figure 3b), which are both enhanced compared to the original OPT. This may be due to the higher efficiency of exciton separation from the heterojunction. In photo on-off switching test, the OPT also presents reproducible photosensing behavior (Figure 3c). As can be seen in Figure 3d, the rise time is reduced from 19.4 to 3.2 s. The fall time (defined as the time for the current to decay to 10% of the maximum value) is also reduced from 6.7 to 0.4 s. It is noteworthy that the on-current increases from 61 nA to 537 nA with about nine times enhancement. In real-time photoresponse test, the *R* and the rise time both decide the on-current value, larger *R* and smaller rise time will lead to higher on-current. The p–n heterojunction enhances the *R* and reduces the rise time, so the on-current is larger. Regarding the maximum measured *R* and *P*, our device presents maximal *R* and *P* as high as 4808 A W^{-1} and 1.7×10^7, respectively.

For making the mechanism of enhancement clear, the device was characterized by atomic force microscope (AFM) and X-ray photoelectron spectroscopy (XPS). As is shown in AFM image (**Figure 4**c), the morphology of PSeTPTI with deposited $PC_{61}BM$ is similar with that of pure PSeTPTI. The $PC_{61}BM$ just makes the surface a little more compact with surface roughness R_q reducing from 2.11 to 1.49 nm. From the XPS results (Figure 4a,b), the surface Se content changes slightly from 1.7% to 1.62%, indicating that the $PC_{61}BM$ does not cover the whole PSeTPTI layer.

Combing the results of AFM and XPS, the $PC_{61}BM$ should have a disperse status on the surface of PSeTPTI just like disperse nanoparticles (Figure 4f). This disperse $PC_{61}BM$ can offer p–n heterojunction but will not form a continuous electron transporting channel which does not influence the OFET behavior and maintains gain mechanism. Figure 4d presents the energy levels (highest occupied molecular orbital (HOMO) and lowest unoccupied molecular orbital (LUMO)) of PSeTPTI and $PC_{61}BM$. From the energy levels, the electrons can transfer from the LUMO of PSeTPTI to the LUMO of $PC_{61}BM$. We also performed the photoluminescence (PL) measurement. The PL intensity is weakened with 3 nm $PC_{61}BM$ compared to the pure PSeTPTI film (Figure 4e). This result also indicates the charge transfer phenomenon between the two materials. In this OPT structure, excitons are also generated in the PSeTPTI but mainly separated in the p–n heterojunction interface. The photogenerated electrons are transferred into disperse $PC_{61}BM$ region very fast and the holes are transported to the drain electrode along the PSeTPTI channel.[29] This is the main photocurrent mechanism. Even though the original process for photoelectrons generated in the PSeTPTI bulk to fill the traps still exists, the generating charge carriers from PSeTPTI/$PC_{61}BM$ heterojunction contribute to most of the photocurrent. As a result, the response speed is not influenced by the original process. Meanwhile, due to the p–n interface to supply a better recombination region, the fall time is also reduced. Summary of detailed performance comparison is listed in **Table 1**.

We also investigated the performance with different $PC_{61}BM$ thicknesses. As shown in **Figure 5**a, the mobility of OFET changes little with 3 nm $PC_{61}BM$, but starting from 5 nm, the mobility decreased about three times compared with device without $PC_{61}BM$. With thicker $PC_{61}BM$, the depletion region of PSeTPTI/$PC_{61}BM$ heterojunction may begin to influence the hole accumulating and transporting in the channel, leading to the decreased mobility. (We also tested the devices

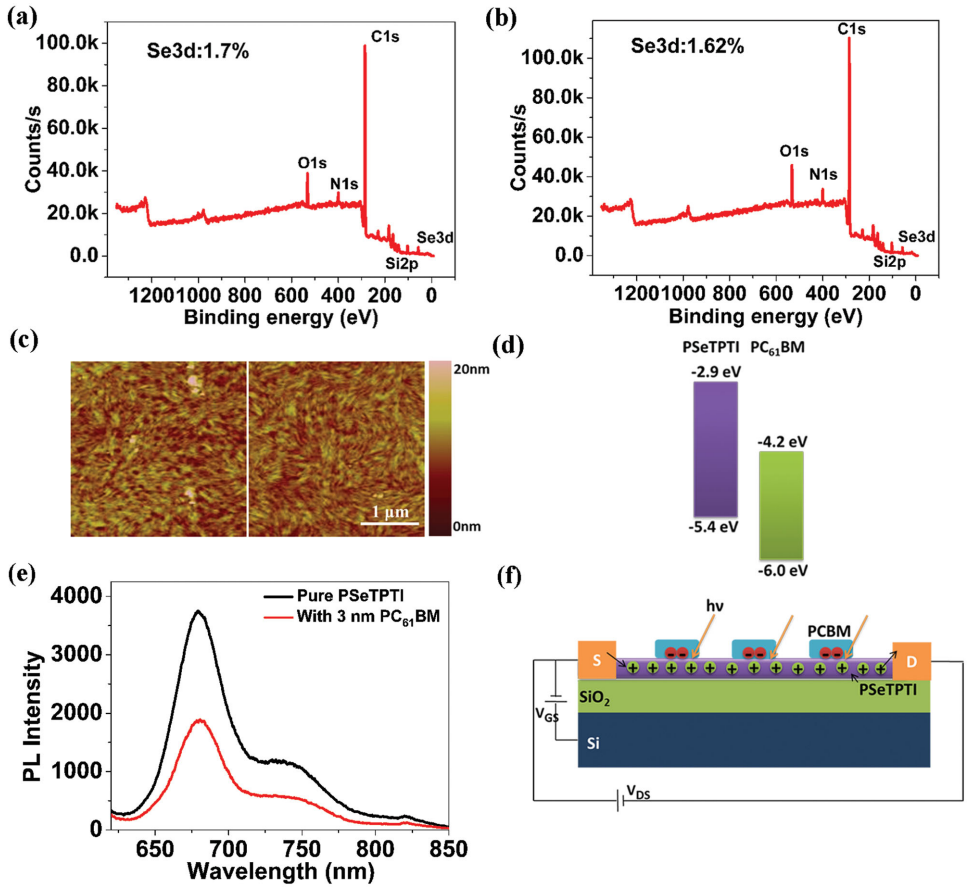

Figure 4. a,b) XPS curves of PSeTPTI thin film without and with 3 nm $PC_{61}BM$. c) AFM images of PSeTPTI without and with 3 nm $PC_{61}BM$ (from left to right). d) Energy levels of PSeTPTI and $PC_{61}BM$. e) Photoluminescence spectra of pure PSeTPTI and PSeTPTI with 3 nm $PC_{61}BM$. f) Schematic of charge separation and transporting process.

without $PC_{61}BM$ after the same storage time, the mobility did not change.) Under illumination, the I_{DS} increases with 3 nm $PC_{61}BM$, due to the introduced p–n heterojunction aforementioned. From 5 to 20 nm, the I_{DS} decreases obviously and becomes lower even than the device without $PC_{61}BM$. By depositing more $PC_{61}BM$, the $PC_{61}BM$ layer probably forms a few continuous electron transporting channels between the source/drain electrodes. From the following equation[30]

$$G = \frac{(\mu_n + \mu_p)\tau E}{L} \tag{3}$$

$$R = \mathrm{EQE}\frac{\lambda e}{hc}G \tag{4}$$

Table 1. Performance comparison of PSeTPTIbased OPTs without and with $PC_{61}BM$ under white light.

Materials	R [A W^{-1}]	P	On-current [nA]	Rise time [s]	Fall time [s]
Pure PSeTPTI	362	1.1×10^5	61	19.4	6.7
With $PC_{61}BM$	1010	2.3×10^5	537	3.2	0.4

where G is the photogain value, L stands for the device channel length, μ_n is the electron mobility, μ_p is the hole mobility, τ is the photocarrier lifetime, E is the electrical field in the device, EQE is external quantum efficiency, λ is the wavelength of incident light, e is the absolute value of electron charge, h is the Planck constant, and c is the light speed. The continuous electron channel will reduce the lifetime of photoelectrons and results in lower G and lower R. Moreover, the mobility also decreases from 5 nm. These factors lead to lower photocurrent though the more $PC_{61}BM$ introduces more p–n heterojunctions.

2.3. High-Performance UV Photodetection

Since UV photodetection is very useful in some important fields like aerospace, military, and biological sensing. We explored the UV photodetection performance of the devices. UV photoresponse test was performed with a 365 nm light source of 43 μW cm^{-2}. Under 365 nm UV illumination, the transfer curve moves upward dramatically due to the increased charge carries density by UV excitation (**Figure 6**a). Based on Equations (1) and (2), R and P are calculated. Moreover, due to monochromatic light, G can be obtained and the normalized detectivity (D^*) can be roughly evaluated (assuming that the

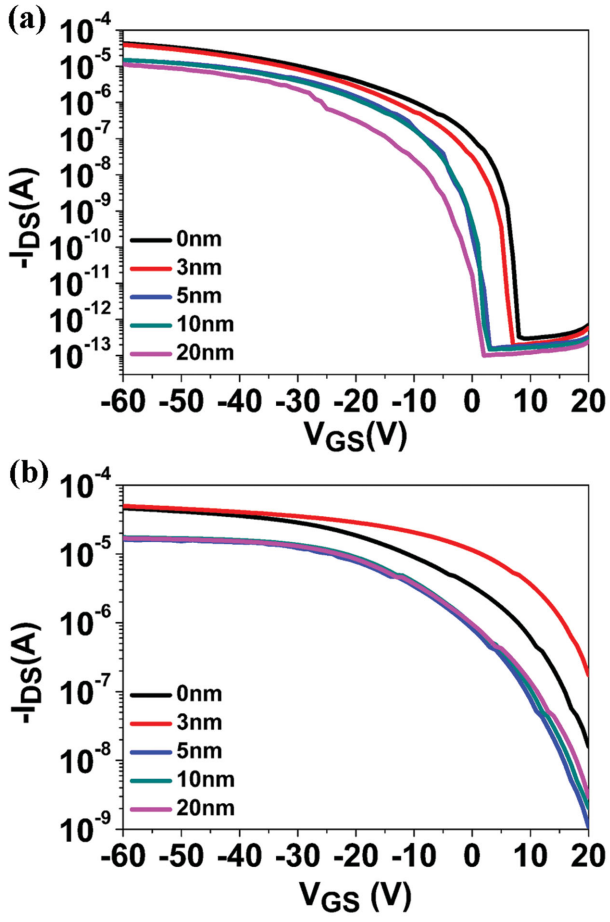

Figure 5. a) Transfer curves with different thicknesses of $PC_{61}BM$ in the dark. b) Transfer curves with different thicknesses of $PC_{61}BM$ under white light illumination.

shot noise from the dark current is the major noise contribution) based on the following equations[12,31]

$$G = \frac{\mathrm{N1(photo\ charges)}}{\mathrm{N2(incident\ photons)}} = \frac{1240 \times (I_{\mathrm{light}} - I_{\mathrm{dark}})}{\lambda(\mathrm{nm}) \times P_{\mathrm{inc}}} \quad (5)$$

$$D^{*} = R(S/2eI_{\mathrm{dark}})^{1/2} \quad (6)$$

where S is the effective area under illumination. As is shown in Figure 6b, the maximum R can be as high as 2.2×10^4 A W^{-1} and P can be 7.3×10^7. At the cross point (V_{GS} = 5.5 V), the R and P are 513 A W^{-1} and 9.6×10^4, respectively. In Figure 6c, the maximum G of the OPTs was nearly 10^5. The D^* of our photodetectors is above 10^{13} Jones and the maximum value was 3.1×10^{16} Jones. At V_{GS} = 5.5 V (the cross point of R and P curves), the G and D^* are 1.9×10^3 and 1.3×10^{15} Jones, respectively. These results indicate the high UV sensitivity of our OPTs.

The real-time photo on/off switching test was also investigated. As can be found in Figure 6a, different V_{GS} will produce different I_{DS} under UV illumination. We studied the real-time photoresponse under different V_{GS} (10, 20, 30, 40 V).

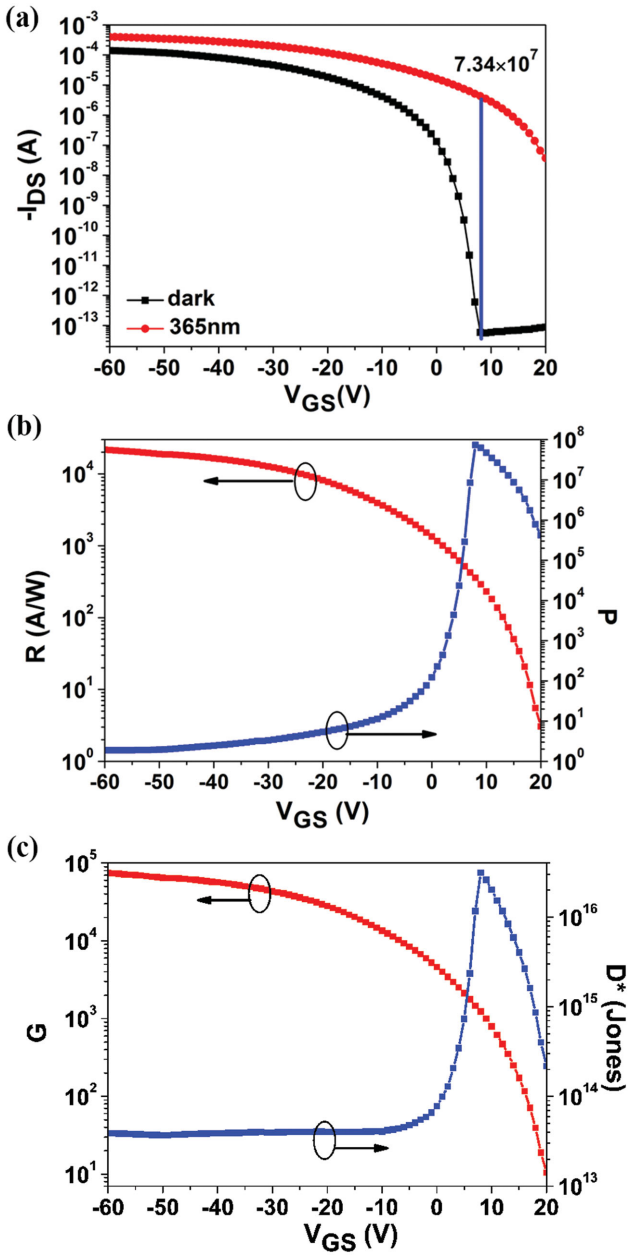

Figure 6. a) Transfer curves in the dark and under 365 nm UV light with 43 μW cm^{-2} intensity. b) R and P as a function of V_{GS}. c) G and D^* as a function of V_{GS}.

Surprisingly, the curves are similar, especially regarding the on-current value (**Figure 7**a–d). This is adverse to anticipation from Figure 6a. In every photoresponse cycle, the PPC phenomenon was also observed indicating the photomemory effect. Figure 7e shows the transfer curves with different starting V_{GS} under UV light. With more positive starting V_{GS}, the threshold voltage moved to a more positive one leading to a higher I_{DS} curve than that with smaller starting V_{GS}. This result is just due to the photomemory effect. The situations are different sweeping from 10 V and from 20 V. The photomemory effect of the previous sweeping region from 20 to 10 V will influence the I_{DS} at 10 V. Thus, under the same V_{GS} of 10 V, the I_{DS} value sweeping from

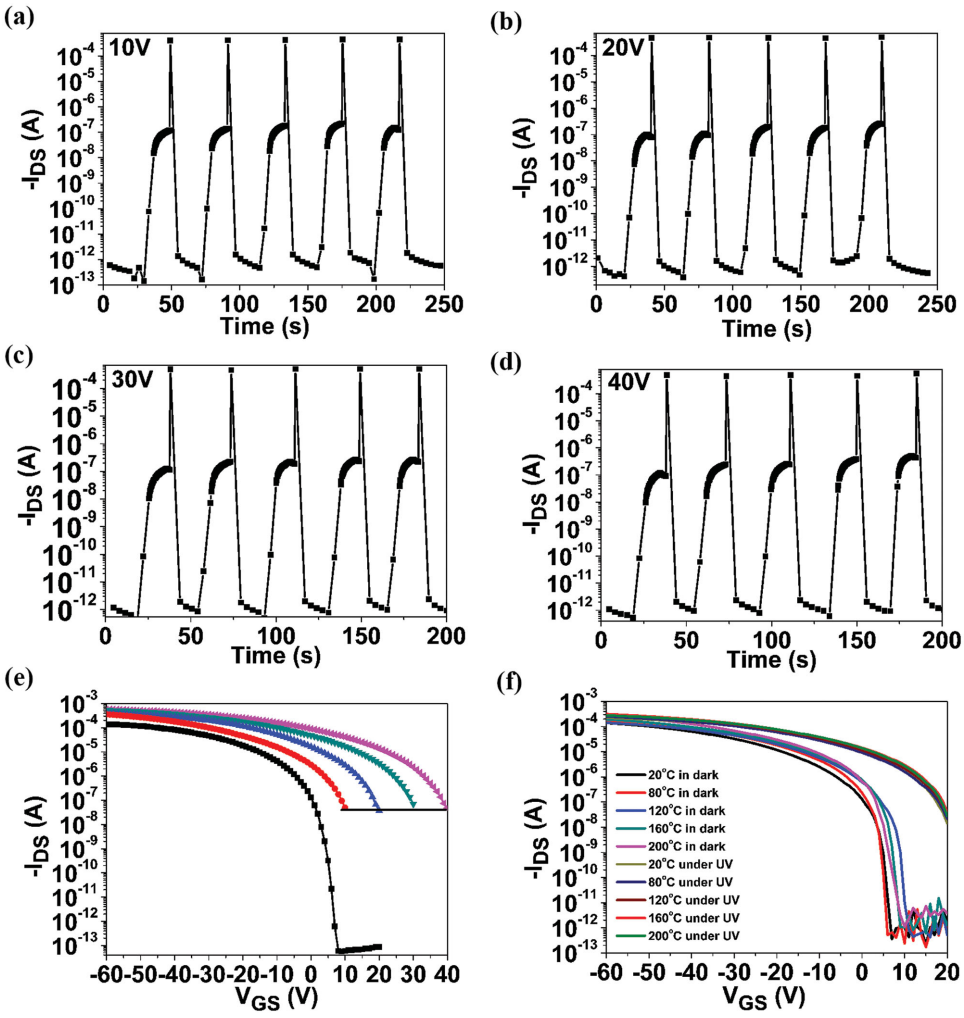

Figure 7. a–d) Real-time photoresponse test under different V_{GS} of 10, 20, 30, and 40 V, $V_{DS} = -60$ V. e) Transfer curves in the dark and under UV light with different starting V_{GS}, $V_{DS} = -60$ V. f) Transfer curves of devices in the dark and under UV light working at different temperatures of 20, 80, 120, 160, and 200 °C.

20 V will be higher than that from 10 V. That means the I_{DS} value at 10 V in transfer curves sweeping from 20 V is not the real-time one and overrated due to the memory effect. As can be seen in Figure 7e, the currents at starting V_{GS} were similar indicating the similar photocurrent in the real-time test (Figure 7a–d).

2.4. Thermally Stable OPTs

For potential applications in harsh environment conditions, we explored the UV photodetection of our OPTs at high temperatures. From the thermogravimetric analysis (TGA) of PSeTPTI and PCBM,[26,32] the decomposition temperatures are both above 400 °C. As known from the previous report, the performance of PSeTPTI based transistors was insensitive to annealing temperature.[26] These factors inspired us to explore the possible application of our devices at high temperature. Figure 7f presents the transfer curves of our OPTs in the dark and under light at different temperatures of 20, 80, 120, 160, and 200 °C (these temperatures refer to the working temperatures and were obtained through a hot plate under the devices). In the dark, the transfer curves are similar and the mobility keeps stable. The temperature independence of mobility was also found in previous reports.[33] As is generally known, for band transporting model of charge carriers, the temperature coefficient is negative ($d\mu/dT < 0$), for hopping transporting model of charge carriers, the temperature coefficient is positive ($d\mu/dT > 0$). The temperature independence indicates that the transport mechanism is intermediate between these two modes of transport.[33] Under UV illumination, the similar mobility will lead to a similar R. Thus, the transfer curves under UV illumination are almost the same (Figure 7f). For demonstrating a practical application, we performed the real-time photoresponse test. **Figure 8**a–d presents the I_{DS} change with several dynamic photo on/off switching under high-temperature conditions. At 80, 120, 160 °C, and even up to 200 °C, the OPT presents reproducible photoresponse behavior. At these high temperatures, the dark currents are all below 10^{-11} A, and the currents under UV light are all above 10^{-7}A, maintaining stable photoresponse performance. This result indicates that our OPTs are capable of stably working under high-temperature conditions.

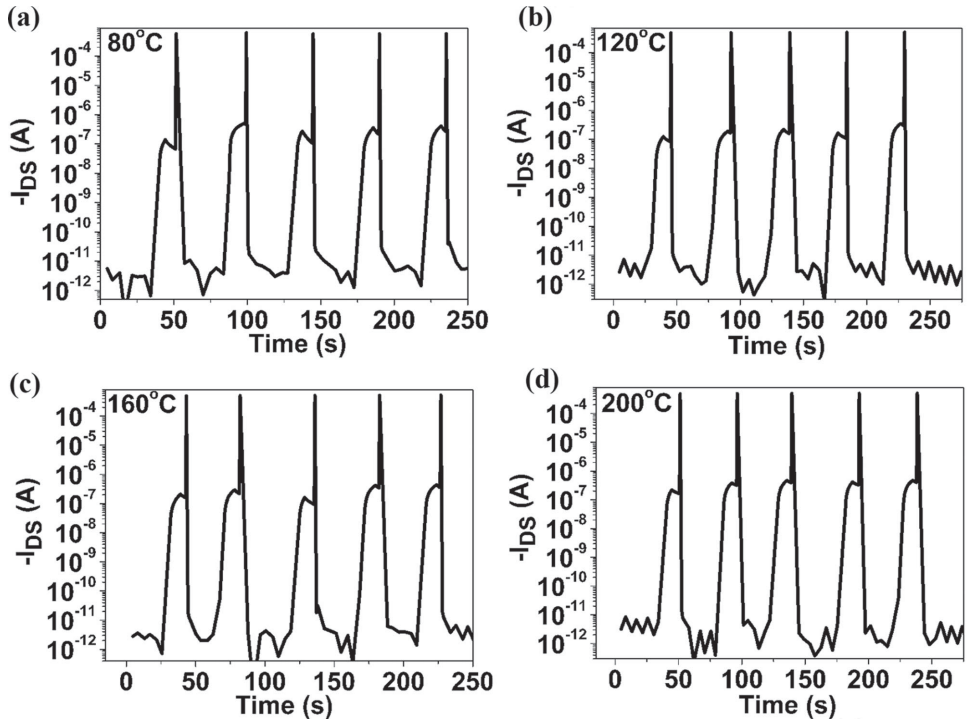

Figure 8. a–d) Real-time photoresponse test of devices working at 80, 120, 160, and 200 °C (V_{GS} = 10 V, V_{DS} = −60 V).

3. Conclusion

In conclusion, donor material PSeTPTI, which has wide light absorption from UV to visible region, was used to fabricate OPTs. The devices show high carrier mobility under ambient conditions with excellent electrical stability. With dispersed $PC_{61}BM$ deposited on the top of the PSeTPTI surface, the photoresponsivity and response speed are both improved as the introduced PSeTPTI/$PC_{61}BM$ heterojunction offers a better mechanism of photocurrent generation and meanwhile the disperse $PC_{61}BM$ does not influence the OFET performance and photogain.

Besides the visible light, the UV photodetection was also investigated. The OPTs present high UV sensitivity with maximum R of 2.2×10^4 A/W, P of 7.3×10^7, G of 7.5×10^4, and D^* of 3.1×10^{16} Jones. Moreover, the OPTs are thermally stable at high temperature even up to 200 °C, showing great potential working at high-temperature environments. Our results here should be very encouraging in exploring high-performance and thermally stable OPTs for multicolor detection.

4. Experimental Section

Device Fabrication: Heavily n-doped silicon was utilized as the common gate electrode and the silicon oxide (300 nm, 10 nF cm^{-2}) acted as the dielectric film. The source and drain electrodes onto the SiO_2 were prepatterned Ti/Au by standard photolithography. The SiO_2 was modified by an octadecyltrichlorosilane (OTS) formed self-assembly monolayer. Then, the PSeTPTI solution with a concentration of 8 mg mL^{-1} was spin coated onto the wafer at 2000 rpm for 30 s with post annealing of 100 °C for just 5 min. All the fabrication processes were performed in air. The $PC_{61}BM$ was thermally evaporated at 0.1 Å s^{-1} under a vacuum pressure of 1×10^{-4} Pa.

Device Characterization: UV–vis spectra were recorded using a JASCO V-570 spectrophotometer. The PL spectra were measured using an F-4500 fluorescence spectrophotometer. A Keithley 4200 semiconductor characterization system was utilized for the electrical test. The white light was offered by a halogen–tungsten lamp and the UV illumination was offered by a UV light. Prior to the utilization of the light, the light intensity was calibrated using a mono-silicon detector. The AFM images were acquired using a Veeco NanoScope IV AFM scanning probe microscope with a silicon cantilever in tapping mode. The XPS measurements were performed in a Kratos Ultra Spectrometer (a base pressure of 1×10^{-9} Torr) using a monochromatized Al Kα X-ray photons ($h\nu$ = 1486.6 eV) discharge lamp.

Acknowledgements

The authors acknowledge the financial support by the 973 Program (Grant Nos. 2014CB643600, 2014CB643503, and 2011CB932304), National Natural Science Foundation of China (61405208), the CAS/SAFEA International Partnership Program for Creative Research Teams, and the Strategic Priority Research Program of the Chinese Academy of Sciences (Grant No. XDB12030200). L.D. thanks the support from the "100 Talents Program" of the Chinese Academy of Sciences and National Natural Science Foundation of China (21374025).

Received: February 7, 2015
Revised: March 18, 2015
Published online: April 13, 2015

[1] H. Yan, Z. Chen, Y. Zheng, C. Newman, J. R. Quinn, F. Dotz, M. Kastler, A. Facchetti, *Nature* **2009**, *457*, 679.
[2] K. J. Baeg, M. Caironi, Y. Y. Noh, *Adv. Mater.* **2013**, *25*, 4210.
[3] D. Natali, M. Caironi, *Adv. Mater.* **2012**, *24*, 1357.

[4] G. A. Salvatore, N. Munzenrieder, T. Kinkeldei, L. Petti, C. Zysset, I. Strebel, L. Buthe, G. Troster, *Nat. Commun.* **2014**, *5*, 2982.
[5] H. T. Yi, M. M. Payne, J. E. Anthony, V. Podzorov, *Nat. Commun.* **2012**, *3*, 1259.
[6] J. Zaumseil, C. L. Donley, J. S. Kim, R. H. Friend, H. Sirringhaus, *Adv. Mater.* **2006**, *18*, 2708.
[7] T. D. Tsai, J. W. Chang, T. C. Wen, T. F. Guo, *Adv. Funct. Mater.* **2013**, *23*, 4206.
[8] Y. Zang, F. Zhang, D. Huang, C. A. Di, Q. Meng, X. Gao, D. Zhu, *Adv. Mater.* **2014**, *26*, 2862.
[9] M. El Gemayel, M. Treier, C. Musumeci, C. Li, K. Mullen, P. Samori, *J. Am. Chem. Soc.* **2012**, *134*, 2429.
[10] H. Usta, M. D. Yilmaz, A. J. Avestro, D. Boudinet, M. Denti, W. Zhao, J. F. Stoddart, A. Facchetti, *Adv. Mater.* **2013**, *25*, 4327.
[11] C. A. Di, F. Zhang, D. Zhu, *Adv. Mater.* **2013**, *25*, 313.
[12] X. Gong, M. Tong, Y. Xia, W. Cai, J. S. Moon, Y. Cao, G. Yu, C. L. Shieh, B. Nilsson, A. J. Heeger, *Science* **2009**, *325*, 1665.
[13] H. Yu, Z. Bao, J. H. Oh, *Adv. Funct. Mater.* **2013**, *23*, 629.
[14] Y. Guo, C. Du, G. Yu, C. A. Di, S. Jiang, H. Xi, J. Zheng, S. Yan, C. Yu, W. Hu, Y. Liu, *Adv. Funct. Mater.* **2010**, *20*, 1019.
[15] M. Y. Cho, S. J. Kim, Y. D. Han, D. H. Park, K. H. Kim, D. H. Choi, J. Joo, *Adv. Funct. Mater.* **2008**, *18*, 2905.
[16] K. J. Baeg, M. Binda, D. Natali, M. Caironi, Y. Y. Noh, *Adv. Mater.* **2013**, *25*, 4267.
[17] K. H. Kim, S. Y. Bae, Y. S. Kim, J. A. Hur, M. H. Hoang, T. W. Lee, M. J. Cho, Y. Kim, M. Kim, J. I. Jin, S. J. Kim, K. Lee, S. J. Lee, D. H. Choi, *Adv. Mater.* **2011**, *23*, 3095.
[18] Y.-Y. Noh, D.-Y. Kim, Y. Yoshida, K. Yase, B.-J. Jung, E. Lim, H.-K. Shim, *Appl. Phys. Lett.* **2005**, *86*, 043501.
[19] T. Pal, M. Arif, S. I. Khondaker, *Nanotechnology* **2010**, *21*, 325201.
[20] X. Wang, K. Wasapinyokul, W. D. Tan, R. Rawcliffe, A. J. Campbell, D. D. C. Bradley, *J. Appl. Phys.* **2010**, *107*, 024509.
[21] K. Wasapinyokul, W. I. Milne, D. P. Chu, *J. Appl. Phys.* **2009**, *105*, 024509.
[22] E. Monroy, F. Omnès, F. Calle, *Semicond. Sci. Technol.* **2003**, *18*, R33.
[23] M. Razeghi, A. Rogalski, *J. Appl. Phys.* **1996**, *79*, 7433.
[24] A. Patra, M. Bendikov, *J. Mater. Chem.* **2010**, *20*, 422.
[25] I. Kang, T. K. An, J. Hong, H.-J. Yun, R. Kim, D. S. Chung, C. E. Park, Y.-H. Kim, S.-K. Kwon, *Adv. Mater.* **2013**, *25*, 524.
[26] J. Cao, S. Chen, Z. Qi, Z. Xiao, J. Wang, L. Ding, *RSC Adv.* **2014**, *4*, 5085.
[27] S. E. Ahn, I. Song, S. Jeon, Y. W. Jeon, Y. Kim, C. Kim, B. Ryu, J. H. Lee, A. Nathan, S. Lee, G. T. Kim, U. I. Chung, *Adv. Mater.* **2012**, *24*, 2631.
[28] Z. Qi, X. Liao, J. Zheng, C. A. Di, X. Gao, J. Wang, *Appl. Phys. Lett.* **2013**, *103*, 053301.
[29] N. S. Sariciftci, L. Smilowitz, A. J. Heeger, F. Wudl, *Science* **1992**, *258*, 1474.
[30] S. M. Sze, K. K. Ng, *Physics of Semiconductor Devices*, Wiley, New York **2007**.
[31] G. Konstantatos, E. H. Sargent, *Nat. Nanotechnol.* **2010**, *5*, 391.
[32] A. Rodrigues, M. C. R. Castro, A. S. F. Farinha, M. Oliveira, J. P. C. Tomé, A. V. Machado, M. M. M. Raposo, L. Hilliou, G. Bernardo, *Polym. Testing* **2013**, *32*, 1192.
[33] W. Mey, A. Hermann, *Phys. Rev. B: Condens. Matter* **1973**, *7*, 1652.